



An hourly shallow landslide warning model developed by combining automatic landslide spatial susceptibility and temporal rainfall threshold predictions

Yi-ming CAO, Wei GUO, Yu-ming WU, Lang-ping LI, Yi-xing ZHANG, Heng-xing LAN

View online: <https://doi.org/10.1007/s11629-022-7370-1>

Articles you may be interested in

[Landslide susceptibility mapping using the infinite slope, SHALSTAB, SINMAP, and TRIGRS models in Serra do Mar, Brazil](#)

Journal of Mountain Science. 2022, 19(4): 1018 <https://doi.org/10.1007/s11629-021-7057-z>

[Impact of geomorphometric parameters on the occurrence and distribution of landslides in Yamuna River Basin, North–Western Himalaya, India](#)

Journal of Mountain Science. 2022, 19(8): 2374 <https://doi.org/10.1007/s11629-021-7081-z>

[Calculation of landslide occurrence probability in Taiwan region under different ground motion conditions](#)

Journal of Mountain Science. 2021, 18(4): 1003 <https://doi.org/10.1007/s11629-020-6540-2>

[Estimation of rainfall thresholds for shallow landslides in the Sierra Madre Oriental, northeastern Mexico](#)


Journal of Mountain Science. 2020, 17(7): 1565 <https://doi.org/10.1007/s11629-020-6050-2>


[A multiobjective evolutionary optimization method based critical rainfall thresholds for debris flows initiation](#)


Journal of Mountain Science. 2020, 17(8): 1860 <https://doi.org/10.1007/s11629-019-5812-1>


Original Article


An hourly shallow landslide warning model developed by combining automatic landslide spatial susceptibility and temporal rainfall threshold predictions



CAO Yi-ming^{1,2}  <https://orcid.org/0000-0002-2523-794X>; e-mail: caoym@lreis.ac.cn

GUO Wei³  <https://orcid.org/0000-0002-7789-2030>; e-mail: guowei7821987@hotmail.com

WU Yu-ming¹  <https://orcid.org/0000-0003-1659-028X>; e-mail: wuym@lreis.ac.cn

LI Lang-ping^{1*}  <https://orcid.org/0000-0001-6398-3161>; e-mail: lilp@lreis.ac.cn

ZHANG Yi-xing⁶  <https://orcid.org/0000-0002-0371-2922>; e-mail: zhangyx@lreis.ac.cn

LAN Heng-xing^{1,4,5*}  <https://orcid.org/0000-0002-7146-932X>;  e-mail: lanhx@igsnr.ac.cn, lanhx@lreis.ac.cn

*Corresponding author

¹ State Key Laboratory of Resources and Environmental Information System, Institute of Geographic Sciences and Natural Resources Research, Chinese Academy of Sciences, Beijing 100101, China

² University of Chinese Academy of Sciences, Beijing 100049, China

³ Fujian Meteorological Service Centre, Fuzhou 350025, China

⁴ School of Geological Engineering and Geomatics, Chang'an University, Xi'an 710064, China

⁵ Key Laboratory of Ecological Geology and Disaster Prevention of Ministry of Natural Resources, Chang'an University, Xi'an 710064, China

⁶ Tianjin University of Commerce, Tianjin 300134, China

Citation: Cao YM, Guo W, Wu YM, et al. (2022) An hourly shallow landslide warning model developed by combining automatic landslide spatial susceptibility and temporal rainfall threshold predictions. *Journal of Mountain Science* 19(12). <https://doi.org/10.1007/s11629-022-7370-1>.

© Science Press, Institute of Mountain Hazards and Environment, CAS and Springer-Verlag GmbH Germany, part of Springer Nature 2022

Abstract: Landslide warning models are important for mitigating landslide risks. The rainfall threshold model is the most widely used early warning model for predicting rainfall-triggered landslides. Recently, the rainfall threshold model has been coupled with the landslide susceptibility (LS) model to improve the accuracy of early warnings in the spatial domain. Existing coupled models, designed based on a matrix including predefined rainfall thresholds and susceptibility levels, have been used to determine the warning level. These predefined classifications

inevitably have subjective rainfall thresholds and susceptibility levels, thus affecting the probability distribution information and eventually influencing the reliability of the produced early warning. In this paper, we propose a novel landslide warning model in which the temporal and spatial probabilities of landslides are coupled without predefining the classified levels. The temporal probability of landslides is obtained from the probability distribution of rainfall intensities that triggered historical landslides. The spatial probability of landslides is then obtained from the susceptibility probability distribution. A case study shows that the proposed probability-coupled model can successfully

Received: 24-Feb-2022

1st Revision: 17-Jun-2022

2nd Revision: 05-Aug-2022

Accepted: 13-Sept-2022

provide hourly warning results before the occurrence of a landslide. Although all three models successfully predicted the landslide, the probability-coupled model produced a warning zone comprising the fewest grid cells. Quantitatively, the probability-coupled model produced only 39 grid cells in the warning zone, while the rainfall threshold model and the matrix-coupled model produced warning zones including 81 and 49 grid cells, respectively. The proposed model is also applicable to other regions affected by rainfall-induced landslides and is thus expected to be useful for practical landslide risk management.

Keywords: Landslide; Hourly warning; Temporal probability; Spatial probability; Rainfall threshold; Susceptibility

1 Introduction

Landslides are one of the major geological disasters leading to many casualties and property losses worldwide (Iverson 2000; Froude and Petley 2018; Lan et al. 2021). Landslide early warning models are currently a commonly utilized tool for managing landslide risks globally. These early warning models can assist local authorities in issuing early warning information regarding future hazards and quickly relocating individuals in high-risk locations to safer places (Stähli et al. 2015; Ju et al. 2015).

Rainfall is among the major landslide-inducing factors (Lan 2003b, 2013), and most landslide early warning models are based on rainfall thresholds derived from conditional links between historical landslides and precipitation data (Marchi et al. 2002; Lan et al. 2004; Giannecchini 2005; Segoni et al. 2018b; Komolvilas 2021). Among these links, the intensity-duration (I-D) threshold has been widely used to forecast the occurrence times of landslides (Caine 1980; Guzzetti et al. 2007; Segoni et al. 2014; Rosi et al. 2021), which focuses only on landslide prediction in the temporal domain. In some studies, the landslide susceptibility map is used for predicting landslides in the spatial domain (Reichenbach et al. 2018; Li et al. 2020), but temporal information about the occurrence of landslides is not considered. In recent years, a growing number of studies have presented the integration and global-scale applications of the two methodologies, showing improvements in the spatial and temporal prediction

capabilities of landslide warnings (Wei 2018; Segoni et al. 2018a; Guzzetti et al. 2020; Ciccacese 2021). To the best of our knowledge, the first trial of regional-scale landslide forecasting by combining rainfall thresholds and the landslide susceptibility (LS) map was conducted based on a hazard matrix (Segoni et al. 2015). In addition, Pradhan et al. (2019) developed a landslide early warning system in which landslide susceptibility classes were integrated with rainfall threshold warning levels, and Monsieurs et al. (2019) developed a new method of determining rainfall thresholds based on antecedent rainfall estimates directly coupled to landslide susceptibility data.

However, those existing coupled methods use a matrix rather than quantitative spatial or temporal landslide probabilities to compute landslide warning levels. The classification of rainfall thresholds and LS levels produces qualitative rather than quantitative warning results, leading to low prediction precision. In addition, hourly landslide warnings are more effective for landslide hazard mitigation than are daily predictions. However, due to limitations regarding data sources, several coupled models (Ahmed et al. 2018; Monsieurs et al. 2019) can produce only daily rather than hourly landslide warnings.

The study proposes an hourly and stably running landslide warning model incorporating quantitative spatial and temporal probabilities. In this paper, the I-D threshold and an automatic modified frequency ratio method (MFRM) are used to quantify the temporal and spatial probabilities, respectively. To meet the requirement of hourly landslide warnings, the parallel method is utilized to reduce the operation time, achieving hourly landslide warnings. The accuracy and improvement of the proposed probability coupled model are evaluated in a case study. Finally, the advantages of the proposed model owing to integrating temporal and spatial probabilities, as well as the applicability of this new model in practice, are discussed. We considered that the proposed hourly probability-coupled model can be easily applied to regions that are frequently impacted by heavy rainfall and can provide practical help for local authorities to efficiently make disaster mitigation decisions.

2 Methodology

The development of the proposed probability-coupled model includes the following three major

steps (Fig. 1): (1) calculation of the temporal probability ($P_{L,T}$); (2) calculation of the spatial probability ($P_{L,S}$); and (3) calculation of the coupled probability (P_L). The coupled landslide occurrence probability (P_L) is obtained simply by multiplying the temporal and spatial probabilities:

$$P_L = P_{L,T} \times P_{L,S} \times 100\% \quad (1)$$

where P_L is the coupled probability ranging from 0% to 100%. The detailed procedures comprised in each major step are described below.

In this study, for the convenience of comparing the warning results output from different models, the warning results of the rainfall threshold model, susceptibility map, matrix-coupled model and probability-coupled model were converted to raster format (pixel units) at a spatial resolution of 1 km. The rainfall data were obtained in Micaps 4 format at a spatial resolution of 1 km × 1 km. The geoenvironmental factors, which were used to generate the susceptibility map, had different spatial resolutions. To match the warnings of the rainfall

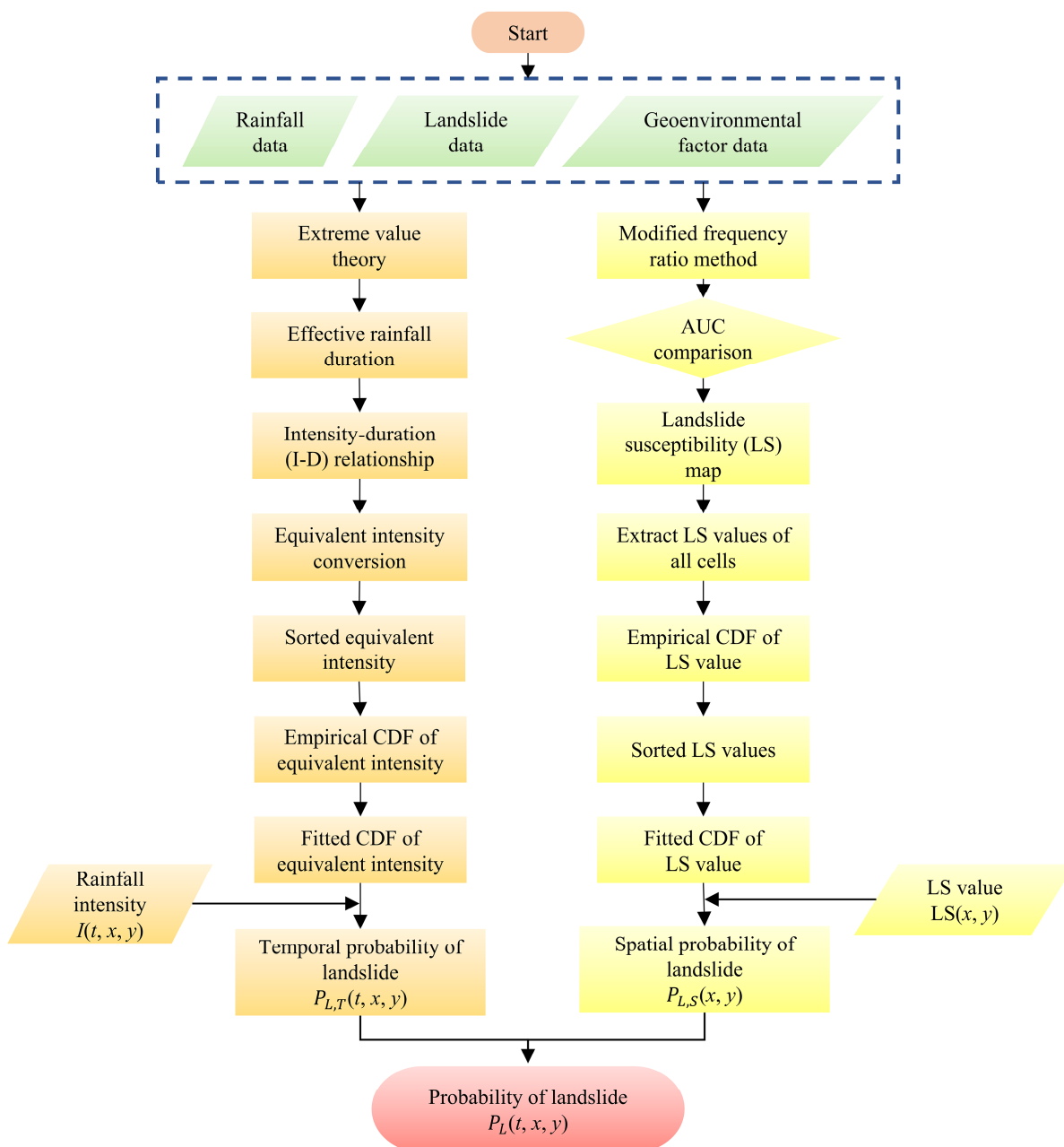


Fig. 1 Flowchart of procedures for calculating temporal and spatial probabilities of landslides.

threshold model, the susceptibility map was resampled with a resolution of 1 km × 1 km by the resampling tool in ArcGIS.

2.1 Calculation of temporal landslide probability

The temporal probability of landslides was calculated herein using the rainfall threshold method, a powerful tool for obtaining regional landslide warnings. The critical I–D threshold concept has been widely used to assess the occurrence of shallow landslides and debris flows all over the world (Caine 1980). The threshold curve is a simple power law relationship that takes the following form:

$$I = AD^{-B} \tag{2}$$

where I is the rainfall intensity of a single rainfall event in millimeters per hour, D is the rainfall duration of that rainfall event in hours, and A and B are empirical parameters.

The prerequisite for establishing a rainfall threshold model is determining the duration of the rainfall process related to the landslide occurrence. A rainfall process may last more than ten days during the plum rain season or for only a few hours during a single rainstorm; thus, determining the effective rainfall process duration can be problematic. In this study, the effective rainfall duration was determined by obtaining the generalized extreme value (GEV) distribution (Fig. 1), which has been shown to be applicable to rainfall events (Jenkinson 1955). For a given rainfall process, based on the hourly rainfall data, the accumulated rainfall value can be calculated by determining the number of hours before the occurrence time of the landslide. The return period can then be obtained for each accumulated rainfall value. The time period corresponding to the maximum return period was used herein as the effective rainfall duration (D) (Floris et al. 2008; Wu et al. 2015). According to the GEV model, the distribution function is given as follows:

$$G_n(CH_{n,j} | \mu_n, \sigma_n, \varepsilon_n) = \exp \left\{ - \left[1 + \varepsilon_n \left(\frac{CH_{n,j} - \mu_n}{\sigma_n} \right) \right]^{-\frac{1}{\varepsilon_n}} \right\} \tag{3}$$

where $CH_{n,j} = \sum_{i=j-n+1}^j H_i$ is the cumulative precipitation over n hours, j is the serial number of the rainfall event that needs to be observed, H_i is the precipitation in hour i , and μ_n , σ_n and ε_n are the

position, scale and shape parameters, respectively. According to the established definition, the return period is the average interval of elements greater than or equal to a certain level during the statistical period of the historical record. Therefore, the return period of a particular rainfall intensity is the average interval between the occurrence of a rainstorm intensity greater than or equal to the selected value. By using the extreme rainfall event distribution function (e.g., Eq. (3)), the extreme rainfall return period (RP) can be calculated as follows:

$$RP(n) = \frac{1}{1 - G_n(CH_{n,j})} \tag{4}$$

where n is the number of hours in the effective rainfall interval and $G_n(CH_{n,j})$ is the cumulative probability of rainfall occurring within n hours of the effective rainfall interval. The number of rainfall hours when the RP reaches its maximum in the selected interval is selected as the effective rainfall duration (D), which can be calculated as follows:

$$D = \arg \max_n (RP(n)) \tag{5}$$

where n is the number of hours in the effective rainfall duration, RP can be calculated from Eq. (4), and D is the effective duration of the rainfall process that induced the landslide. Then, the average hourly rainfall intensity (I) during the effective rainfall duration can be calculated. The two parameters A and B are calculated by obtaining logarithmic transformations on D and I :

$$\log I = \log A + (-B \log D) \tag{6}$$

Then, the best-fitting line in the log-log plot is obtained based on the empirical data of D and I (Fig. 1), thus defining parameter B . We supposed that the best-fitting line represents the trend of the relationship of all rainfall intensities that triggered landslides during the reference rainfall duration. Then, every landslide point was converted to the reference rainfall duration (Fig. 2a) using the slope of the best-fitting line. The parameter A can be defined as the lower bound of the rainfall-induced landslide event points in the graph. Therefore, the equivalent rainfall intensity points can be obtained over the rainfall duration; this step represents the preparation for the next calculation.

The probability distribution of landslide-triggering rainfall intensities, i.e., the distribution of the temporal probability of landslides occurring, is derived based on an equivalency conversion of the

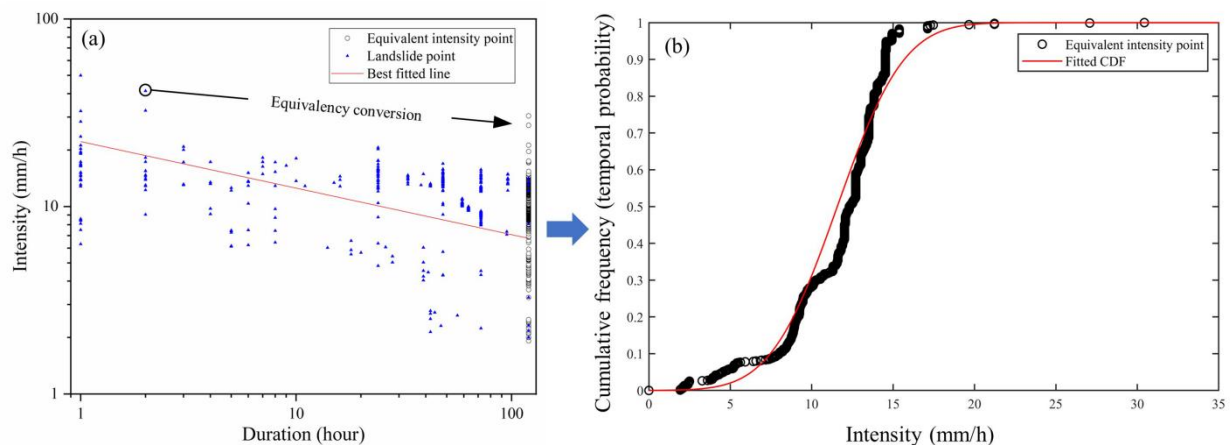


Fig. 2 Temporal probability distribution. (a) the I-D relationship and the equivalency conversion of rainfall intensities that triggered landslides; (b) the empirical and fitted CDF (red curve) of equivalent rainfall intensities.

rainfall intensity (Fig. 1). A reference rainfall duration is first defined such that it is larger than all empirical effective rainfall durations. All rainfall-induced landslide event points exhibit varying rainfall durations on the I-D graph (Fig. 2a). The best-fitting line in the I-D graph represents the trend of the relationship of all rainfall-induced landslide event points. Then, a dataset containing the landslide points identified under the same rainfall duration converted by the slope of the best-fitting line can be calculated. We assumed that all landslides were induced by rainfall processes with the same rainfall duration but that the equivalent-occurrence rainfall intensity values varied. An empirical cumulative distribution of all equivalent rainfall intensities triggering landslides was then obtained after sorting these values from low to high. Then, as shown in Fig. 2b, the equivalent rainfall intensity points were plotted as scatter plots in the coordinate space, with the vertical axis representing the rainfall intensity (I) and the horizontal axis representing the cumulative frequency (i.e., temporal probability). Finally, a cumulative distribution function (CDF) of the equivalent rainfall intensities was fitted to the normal distribution. The temporal probability of triggering a landslide (i.e., $P_{L,T}$) under a certain rainfall intensity within the reference rainfall duration could then be obtained from this fitted CDF (Fig. 2b).

2.2 Calculation of spatial probability

The spatial probability of a landslide occurring was calculated herein using the LS, as this metric denotes the relative possibility of a future landslide

occurring in a given spatial domain. Data-driven LS assessment methods have been extensively studied (Guzzetti et al. 1999; Cachon et al. 2006; Corominas 2014), including the frequency ratio (FR) (Aditian 2018; Li et al. 2017; Sharma et al. 2018), weight of evidence (Kayastha et al. 2012; Roy 2019; Torizin et al. 2022), certainty factor model (Lan et al. 2004), fuzzy logic (Vakhshoori et al. 2016; Zhang et al. 2022), information value (Wang et al. 2015; Ghobadi 2017), artificial neural network (Choi et al. 2012; Hong et al. 2020), support vector machine (Huang 2018) and random forest methods (Youssef et al. 2016; Chapi et al., 2017; Liao et al. 2022).

The frequency ratio method is widely employed by researchers due to its simplicity and clarity (Zhang et al. 2020). In the traditional frequency ratio method, landslide-related geoenvironmental factors with continuous values are classified before the frequency ratio value is calculated using various classification methods, such as natural breaks (Jaafari et al. 2014; Ozturk et al. 2022), equal intervals (Chen et al. 2017) and manual methods. Assuming that D and F represent specific geological disasters and geoenvironmental factors, respectively, first, F is grouped into several types or classes as F_i ($i = 1, 2, 3, \dots, m$); then, the FR value of each type or class corresponding to this factor is calculated as follows:

$$FR_i = \frac{P(DF_i)}{P(F_i)} \quad (7)$$

where $P(DF_i)$ is the frequency of F_i in D and $P(F_i)$ is the frequency of F_i in the study area. Summing the frequency ratios obtained for different factors gives the landslide susceptibility index (LSI) value:

$$LSI = \sum_j^n FR_i^j \quad (8)$$

where j ($j = 1, 2, 3, \dots, n$) is the ID of each geoenvironmental factor and FR_i^j is the frequency ratio of the i th type or class of the j th factor.

However, inconsistency and subjectivity problems associated with the traditional frequency ratio method arise as a result of the categorization of geoenvironmental factors. To address this issue, MFRM and an automatic GIS extension called “Automatic Landslide Susceptibility Assessment” (ALSA) were proposed by Li et al. 2017; this method consists of three basic procedures: normalization, precision setting, and frequency statistics. The modified method does not require that the classification of geoenvironmental factors be executed with continuous values. Therefore, the modified method does not provide frequency ratios for only a limited number of factor classes but provides these ratios for all identical normalized factor values (Li et al. 2017). In this way, many more LS values can be obtained, thus facilitating the generation of the LS probability distribution.

An empirical cumulative distribution of the calculated LS values can be obtained after sorting these values, similar to the procedures applied to derive the temporal landslide probability (Fig. 1). Then, the CDF of the LS values can be fitted to a normal distribution (Fig. 1). The spatial probability of triggering a landslide (i.e., $P_{L,S}$) under a certain LS value can then be obtained from this fitted CDF. The susceptibility map and the corresponding CDF remain unchanged until the landslide inventory and geoenvironmental factor data are updated.

2.3 Criterion for coupled warnings

A spatiotemporally comprehensive probability (i.e., P_L) was calculated by coupling $P_{L,T}$ and $P_{L,S}$ according to Eq. (1). The coupled probability was then used to issue landslide warning levels (“very low”, “low”, “moderate”, “high” or “very high”) according to the criteria shown in Fig. 3. A light-blue alert (i.e., very low) indicates that the probability of a landslide occurring is very low, while a red alert (i.e., very high) indicates that the potential for a landslide occurring is enormous; in this situation, the immediate implementation of efficient risk mitigation measures is expected.

3 Case Study

3.1 Study area and data

Nanping city, located in Fujian Province, Southeast China, was chosen as the study area in this research (Fig. 4). This city has a population of approximately 2.68 million people and occupies 26,300 km², comprising one-fifth of Fujian Province. Hills and low mountains occupy approximately 80% of this area, and the terrain is high in the northeast and low in the southwest, spanning the Wuyi Mountains, Shanling Mountains, Xianxialing Mountains, and Jiufeng Mountains. The residual-slope soil layer is widely developed and thick in this area. The geological environment is fragile, and planes of weakness are widespread. The southern study area is dominated by metamorphic rocks; the center contains Mesozoic volcanic rocks and sedimentary rocks, whereas the northern region is composed of granite. The forest coverage rate reaches 75%, and the forest types include evergreen needleleaf forests, evergreen broadleaf forests, and economic forests. There are also abundant water systems in the

| | | | | | |
|-----------------------|------------|-----------|-----------|----------|----------|
| Probability (P_L) | 90.1%~100% | 50.1%~90% | 10.1%~50% | 1.1%~10% | 0~1% |
| Warning level | Very High | High | Moderate | Low | Very Low |

Fig. 3 Criterion for classifying landslide warning levels based on value of landslide probability (P_L).

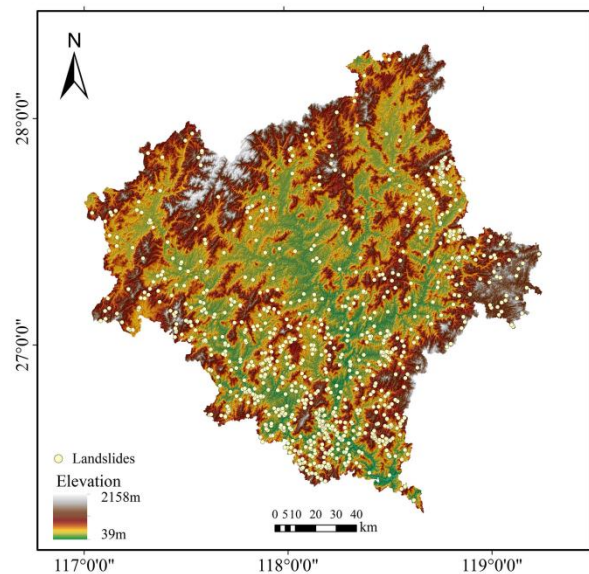


Fig. 4 Landslide inventory of Nanping, Fujian Province, China used in this study.

study area, mainly including one river, the Minjiang River, and eight stream systems. The study area has a typical subtropical humid monsoon climate. The annual average temperature is 17°C, and the average precipitation amount ranges between 1400 and 2000 mm each year. Nanping suffers from typhoons and short-term heavy rainfall, especially during the rainy season, which lasts from May to September. Short-term heavy rainfall is the main factor causing landslides in the study area.

Table 1 shows detailed information about the data used in this study. The landslide inventory utilized herein (Fig. 4) contains a total of 912 landslides that occurred in the period from 2010 to 2019. These landslides were reported to the emergency agency by local residents. The inventory records the occurrence time, location information (e.g., specific address and coordinates), type, volume, and lithology of each landslide. Rock slides (mainly consisting of granite and metamorphic sandstone) accounted for 6.9% of all events, while soil slides (mainly involving residual-slope soils and sandy clay soils) accounted for 79.3%. These rainfall data were produced through multisource data fusion methods, including observation data collected from rainfall stations (256 stations in the study area), radar-derived rainfall data, and satellite-based precipitation products (e.g., precipitation data provided by the rainfall products of the Fengyun-2 satellite). These rainfall data are available at a temporal resolution of one hour and a spatial resolution of 1 km. The period of this rainfall data product spans from 2010 to the present, thus covering the occurrence times of all landslides in the inventory used herein. These real-time rainfall data are provided hourly.

Table 1 Detail information about dataset

| Parameters | Original data format | Converted data format | Resolution (Original data) | Resolution (Converted data) | Data source |
|------------------|------------------------------------|-----------------------|--|--|--|
| Landslides | Excel files (Detailed information) | Shapefile (Point) | - | - | Fujian Meteorological Service Centre (FMSC) |
| Rainfall | Micaps 4 | ASCII file | 1 km (spatial resolution) 1 h (temporal resolution) | 1km (spatial resolution) 1h (temporal resolution) | FMSC (Production of multi-source data fusion) |
| DEM | Raster | Raster | 90 m | 1 km | Geospatial Data Cloud website |
| Lithology | Shapefile (Polygon) | Raster | 1:20,0000 | 1 km | GeoCloud database of the China Geological Survey |
| Soil thickness | Shapefile (Polygon) | Raster | 1:20,0000 | 1 km | FMSC |
| Geomorphic types | Shapefile (Polygon) | Raster | 1:140,0000 | 1 km | GeoCloud database of the China Geological Survey |
| Faults | Shapefile (Polyline) | Raster | 1:20,0000 | 1 km | GeoCloud database of the China Geological Survey |

3.2 Results

3.2.1 Temporal probability distribution

The I-D relationship was derived in this work based on the 912 historical landslides recorded in the utilized landslide inventory and their corresponding rainfall processes. The effective rainfall duration (D) and corresponding rainfall intensity (I) of each historical landslide were plotted on a log-log graph, and a best-fitting line was defined through linear regression (Fig. 2a). In this study, a maximum effective rainfall duration of 120 hours was selected as the reference rainfall duration to determine the rainfall threshold. Then, the equivalent landslide-triggering rainfall intensities were calculated with regard to the reference rainfall duration for each historical landslide (Fig. 2a). The obtained empirical and fitted CDFs of the equivalent rainfall intensities are shown in Fig. 2b. The maximum equivalent rainfall intensity that triggered a landslide was 30.4 mm/h; therefore, the probability of a rainfall intensity equal to or larger than this value triggering a landslide would be considered 100%. The warning results produced by the traditional rainfall threshold model could be obtained by the classified warning levels based on the equivalent rainfall intensity. To maintain consistency, the warning level of the rainfall threshold has the same grading criteria as the proposed probability coupled model (Fig. 3). It should be mentioned that this I-D relationship and the corresponding CDF should be updated when new landslides occur.

3.2.2 Spatial probability distribution

The LS in the study area was evaluated using

eight landslide-related geoenvironmental factors, namely, elevation, slope, aspect, profile curvature, lithology, soil thickness, geomorphology, and distance to fault (Fig. 5). The four topographic factors, including the elevation, slope, aspect, and profile curvature, were derived from the terrain data at a spatial resolution of 90 m. The other four factors, including the lithology, distance to fault, geomorphology, and soil thickness, were derived from vector maps at a 1:20,000 scale. The elevation data of Nanping city were obtained from the SRTM at a resolution of 90 m. The terrain in the study area is high in the northwest, southwest, and eastern border areas, while the central region contains scattered plains and hills (Fig. 5a). The slope values range from

0° to 77.6°. The slopes are steeper in the northwest, southwest, and east areas and gentler in the central region; this distribution is consistent with the spatial elevation distribution (Fig. 5b). The aspect is expressed in positive degrees from 0° to 360°, measured clockwise from the north direction. The flat cells in the input raster (cells with slopes of zero) were assigned an aspect of -1 (Fig. 5c). The curvature values ranged from -0.09 to 0.11 (Fig. 5d). A positive value indicates that the surface is upwardly convex at the plan curvature cell. A negative plane indicates that the surface is upwardly concave at that cell. A value of 0 indicates that the surface is flat. Eight different geological lithology types were classified by ranking the hardness from high to low, including granodiorite,

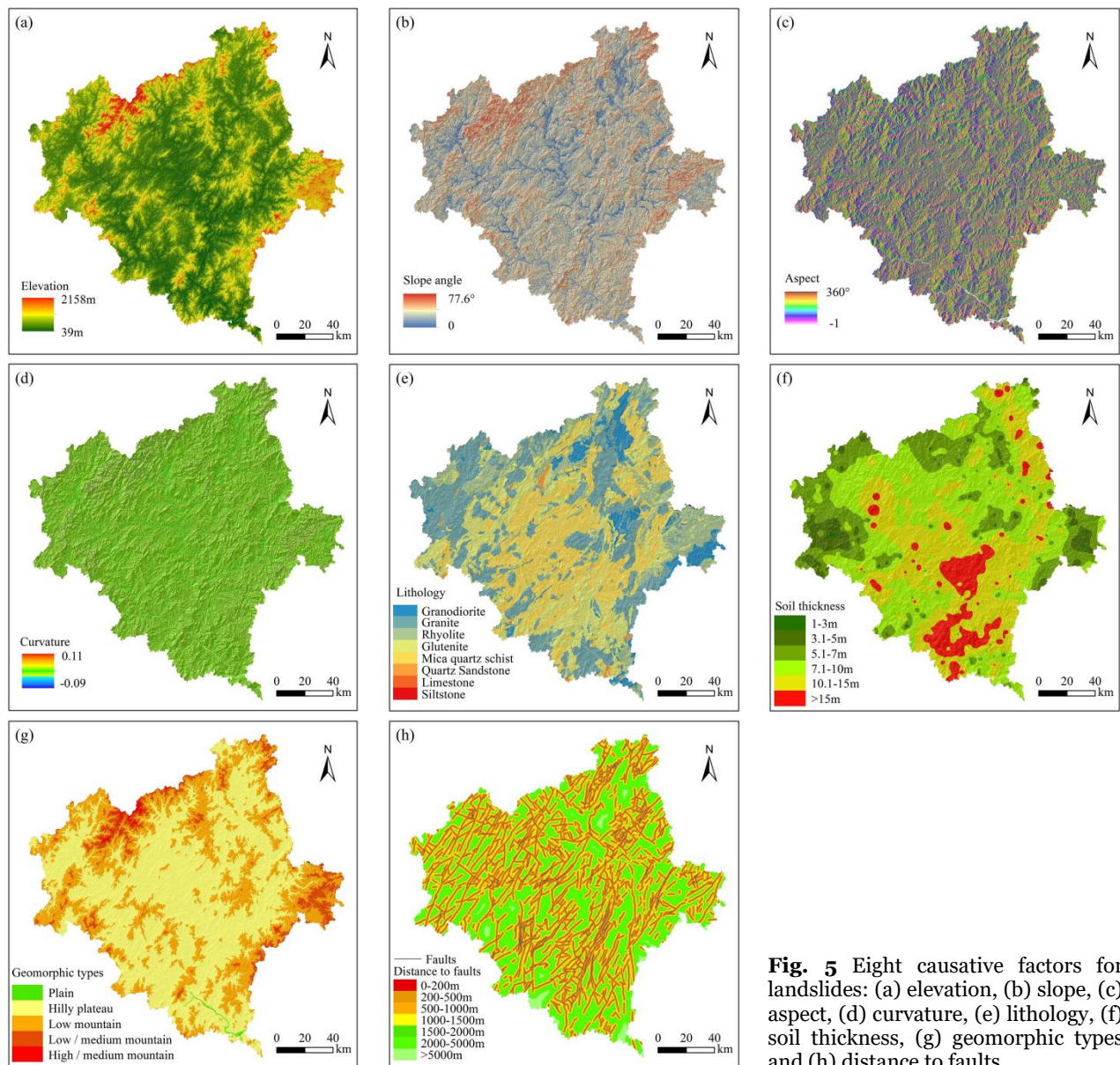


Fig. 5 Eight causative factors for landslides: (a) elevation, (b) slope, (c) aspect, (d) curvature, (e) lithology, (f) soil thickness, (g) geomorphic types and (h) distance to faults.

granite, rhyolite, glutenite, mica quartz schist, quartz sandstone, limestone, and siltstone (Fig. 5e). Six grades were classified in the surface soil depth map. The larger the depth value was, the greater the depth grade was (Fig. 5f). We divided the geomorphic types into five categories: plains, hilly plateaus, low mountains, low and medium mountains, and high and medium mountains (Fig. 5g). The distance to faults was divided into seven classes. The closer the distance to a fault was, the greater the effect on potential landslides was (Fig. 5h).

To increase the objectivity of our evaluation and obtain a more reliable landslide susceptibility map, comparisons were made among various methods. In recent years, machine learning has become one of the most popular approaches to assessing landslide susceptibility. Therefore, landslide susceptibility maps have been produced using machine learning methods, e.g., Artificial Neural Network (ANN) and

MFRM (Fig. 6). The landslide points were regarded as the landslide dataset, and an equal number of nonlandslide points were randomly generated from the grid cells of the study area. Both the landslide dataset and nonlandslide dataset were randomly split into 80% to be used for data training and 20% to be used for data testing (Di Napoli et al. 2020) by using the ArcGIS tool “Subset Features”. Both of these susceptibility maps were normalized to facilitate a more objective comparison, and the findings showed that the vast majority of landslides occurred in areas with relatively high susceptibility values. The central and southwestern parts of the study area showed relatively high susceptibility levels in both maps, while the northwestern and eastern areas showed lower susceptibility levels. However, the susceptibility level of the western area was higher in the ANN map than in the MFRM map. Overall, the highest and lowest susceptibility values accounted for the vast

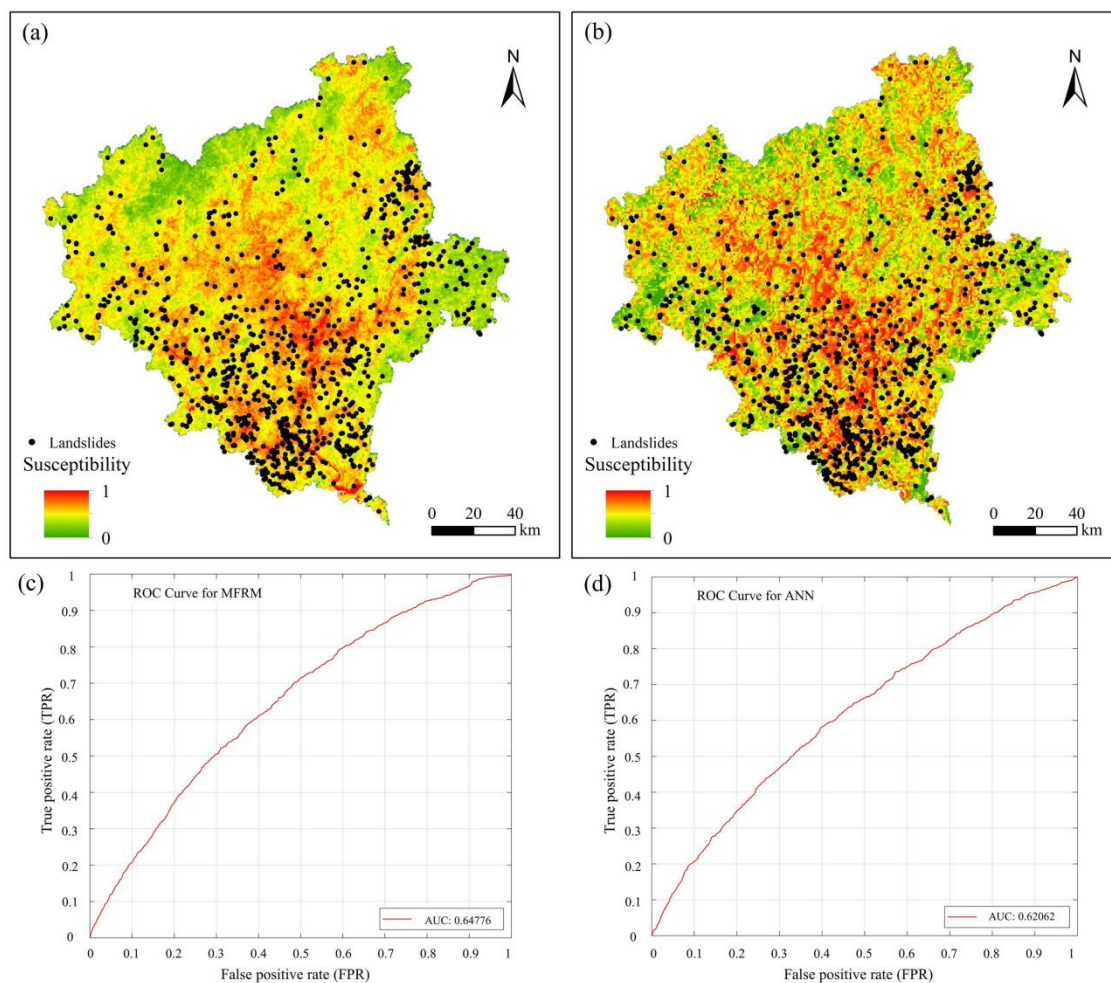


Fig. 6 Normalized landslide susceptibility map and AUC of different methods: (a) susceptibility map of MFRM, (b) susceptibility map of machine learning method (ANN), (c) AUC result of MFRM, (d) AUC result of ANN.

majority of the study region in the ANN map (Fig. 6b), meaning that the number of median-susceptibility values in this map was excessively small, leading to overly high or low warning level results.

A Kolmogorov–Smirnov (KS) test was used for statistical significance, and the p value was used to determine the probability of rejecting the null hypothesis as a result of hypothesis rejection. A p value < 0.05 indicates that the null hypothesis must be rejected, indicating a statistically significantly different algorithm (Ma et al. 2022). The susceptibility values of ANN and MFRM were normalized prior to the statistical significance test (Table 2). The p value was 2.706×10^{-15} , which was much lower than 0.05 and clearly indicated statistical significance. The receiver operating characteristic (ROC) curve and the area under the ROC curve (AUC) of the success rate and prediction rate are frequently used to assess the performances of landslide susceptibility methods (Sala et al. 2021). The closer the AUC value is to 1, the more perfect the method is. The AUC of the ANN susceptibility map was 0.621 , while that of the modified frequency method was 0.648 (Fig. 6c, d). The AUC result of the modified frequency method was slightly higher than that of the ANN method. This finding may have been due to the characteristics of the landslide point data used in the study; one landslide represented only one raster pixel. This number of landslide pixels was thus too small considering the more than thirty thousand raster pixels in the study area. Therefore, the ANN method may not be the most advantageous method. One of the benefits of the FR method is that it allows variations in individual geoenvironmental factors to

be considered in landslide susceptibility assessments. The weight values of all these factors can be conveniently adjusted according to the actual changes in the local geoenvironmental conditions.

This modified method prevents the subjective classification of geoenvironmental factors with continuous values; thus, this method was utilized herein. The minimum and maximum susceptibility values were 0.47 and 46.5 , respectively (Fig. 7b). The obtained empirical and fitted CDFs of the LS values are shown in Fig. 7c. Then, the probability of a given LS value triggering a landslide, i.e., the spatial probability of a landslide occurring (P_{LS}), was obtained from the continuous fitted CDF (Fig. 7c). Similarly, when landslide data are updated, an update of the susceptibility map is also recommended.

Table 2 Descriptive statistics of normalized susceptibility values and the p value of KS test

| Parameter | Artificial neural network (ANN) | Modified frequency ratio method (MFRM) |
|----------------|---------------------------------|--|
| Count | 33441 | 33441 |
| Mean | 1.79348×10^{-13} | -2.39181×10^{-12} |
| Std. deviation | 1.00003×10^0 | 1.00003×10^0 |
| Minimum | -2.79074×10^0 | -5.58586×10^0 |
| Maximum | 3.23647×10^0 | 1.00564×10^1 |
| P value | 2.706×10^{-15} | |

3.3 Validation

A random sample of the utilized landslide datasets was divided into two sets: a training set and a test set; this division represents a conventional method used to test the performances of models (Brunetti et al. 2021). To test the performance of the model developed herein, we randomly split the

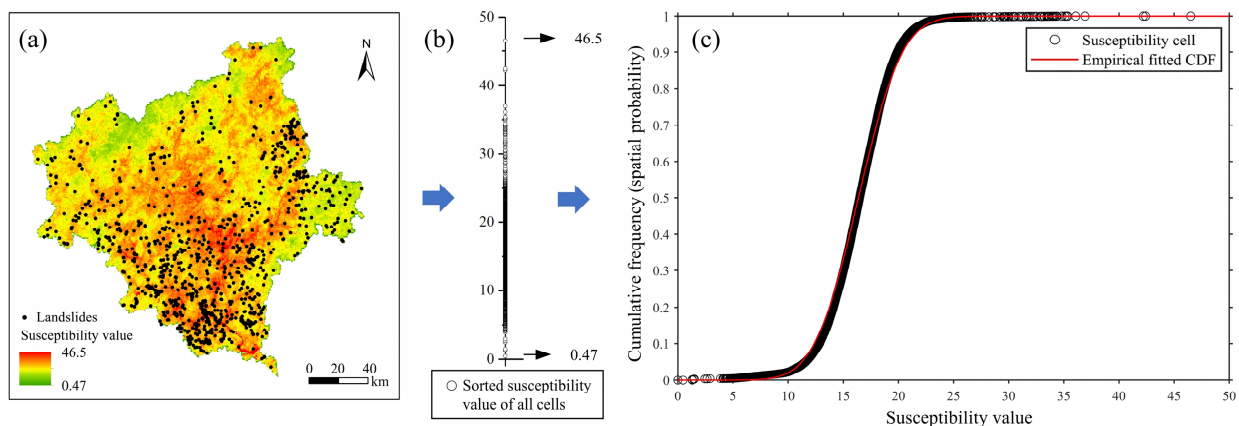


Fig. 7 Spatial probability distribution. (a) LS map; (b) the sorted susceptibility value of all cells; (c) the empirical and fitted CDF (red curve) of susceptibility values.

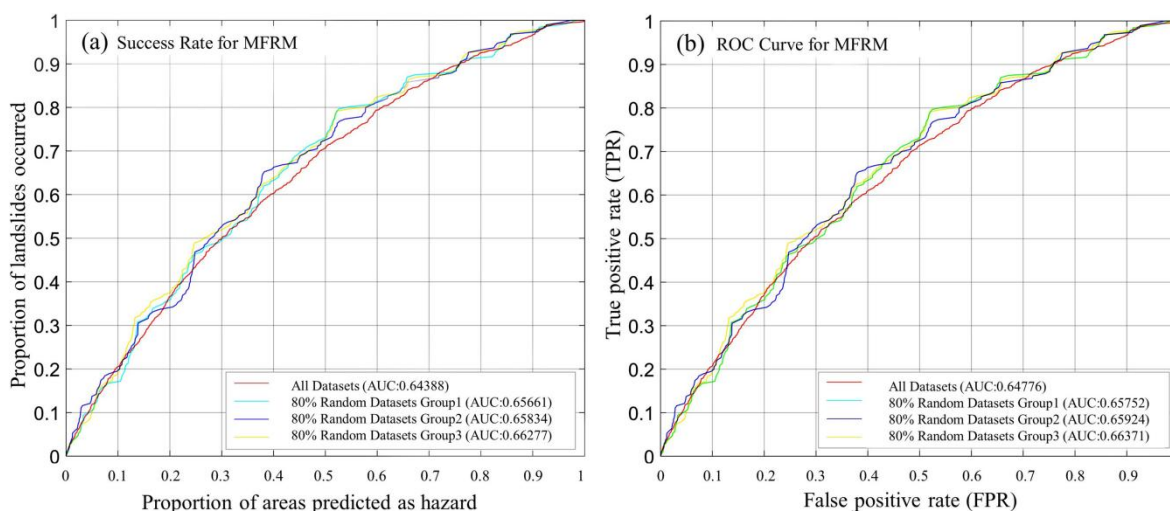


Fig. 8 Success rate and ROC curve for MFRM with different four groups of datasets. (a) Success rates; (b) ROC curves.

landslide dataset into two parts by using the ArcGIS tool “Subset Features”, with 80% being used as training data and 20% as testing data. Eighty percent of the landslide dataset was used to build the susceptibility map with the MFRM, while 20% of the landslide dataset was used to validate the performance of this method. Three iterations were conducted with different groups of random datasets to perform a validation procedure. Fig. 8 shows the success rate and ROC curve of the MFRM with all three 80% random dataset groups and all datasets. The AUC values of these four dataset groups varied little, indicating that the performance of the MFRM susceptibility assessment was both stable and applicable.

The proposed probability-coupled model was validated based on a landslide inventory containing 40 landslides that occurred from January to May 2021. The warning results were classified into three categories, including successful warnings, false warnings and failed warnings (Fig. 9). A warning result was considered successful if the corresponding landslide points were located in “high” or “very high” warning level areas, while a warning result was considered false when the landslide-point regions were not captured by either of these two warning levels. If a warning result corresponded to the “high” or “very high” warning level when no landslide occurred, it was considered a failed warning. As shown in Fig. 9, 33 landslides were successfully captured in the warning results, accounting for 82.5% of all landslides in the inventory, while 7 landslides occurred without warning. Most of these failed

warnings occurred in January, February, and March. This was likely because rainfall is minimal in the first three months of the year and gradually begins to increase starting in April, and the proposed probability-coupled model is strongly governed by the rainfall conditions. This may result in false alarms, as there is now more rainfall in May than in the previous months.

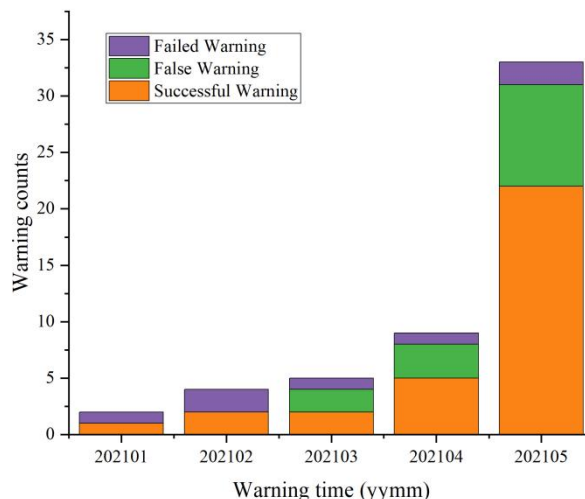


Fig. 9 Warning results based on the probability coupled model from January to March 2021.

The proposed probability-coupled model was tested using the typical Raoba landslide that occurred in Nanping, which has a longitude and latitude of 117°44'47"E and 27°16'39"N at 12:05 on 28 June 2021 (Fig. 10a). The main body of this landslide was approximately 50 m - 60 m wide, and its axial length was approximately 65 m. The volume of the slump

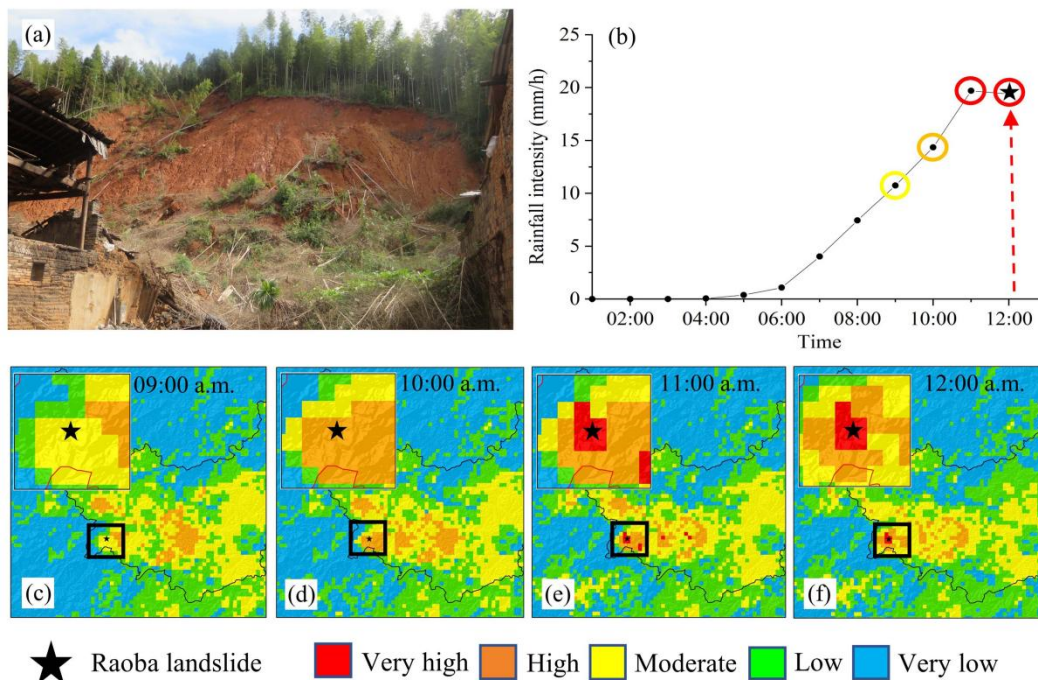


Fig. 10 Validation of the model. (a) the Raoba landslide photographed during the field investigation, view from east; (b) hourly rainfall intensity before the occurrence of the landslide; (c) warning result at 9:00 (moderate); (d) warning result at 10:00 (high); (e) warning result at 11:00 (very high); (f) warning result at 12:00 (very high).

soil was approximately 8000 m³. The slope surface was composed of residual cohesive soils with depths of 2 m - 3 m. The slope failure was induced by short-term heavy rainfall according to the field investigation and rainfall record. In particular, the hourly rainfall intensity peaked at 19.4 mm/h at 11:00 (Fig. 10b). The continuous infiltration of surface water in the slope destroyed the original equilibrium stress state of the slope.

The warning levels in different hours provided by the probability-coupled model suggest that the Raoba landslide region was in a moderate-alert zone at 9:00 (Fig. 10c). The model predicted that at 10:00, the Raoba landslide region became a high-alert zone (Fig. 10d), and at 11:00, it became a very-high-alert zone (Fig. 10e). At 12:00, although the rainfall intensity value was lower than that recorded at 11:00, the model predicted that the Raoba landslide region was still in a very-high-alert zone (Fig. 10f). This case suggests that the proposed probability-coupled model can successfully provide informative hourly warnings before the occurrence of a landslide.

4 Discussion

4.1 Advance of probability coupled model

Landslide risk management is thus difficult owing to uncertainties in both the temporal and spatial probabilities of landslides (Lan 2003a). Rainfall threshold models focus on the temporal probability of landslides occurring. However, landslides are also influenced by geoenvironmental factors, which determine the spatial probability of landslides occurring. Therefore, a landslide warning model in which temporal and spatial probabilities are coupled may be advantageous in integrating the spatial probability of landslides.

A landslide warning model that couples spatial and temporal probabilities was created herein based on coupling the rainfall threshold model with the LS map. In recent years, some researchers have tried to propose a version of the matrix model wherein the matrix is calibrated with objective criteria (Segoni et al. 2018a; Wei et al. 2018; Ahmed et al. 2018; Pradhan et al. 2019). Before the landslide warning level calculation of the matrix, the results of the rainfall threshold and the LS assessment were classified into different grades. Although the matrix operation calculates a warning result, it may not be truly representative of the probability of landslides. In addition, the subjectivities inherent in the manual classification of rainfall thresholds and the LS assessment will affect the accuracy of the landslide

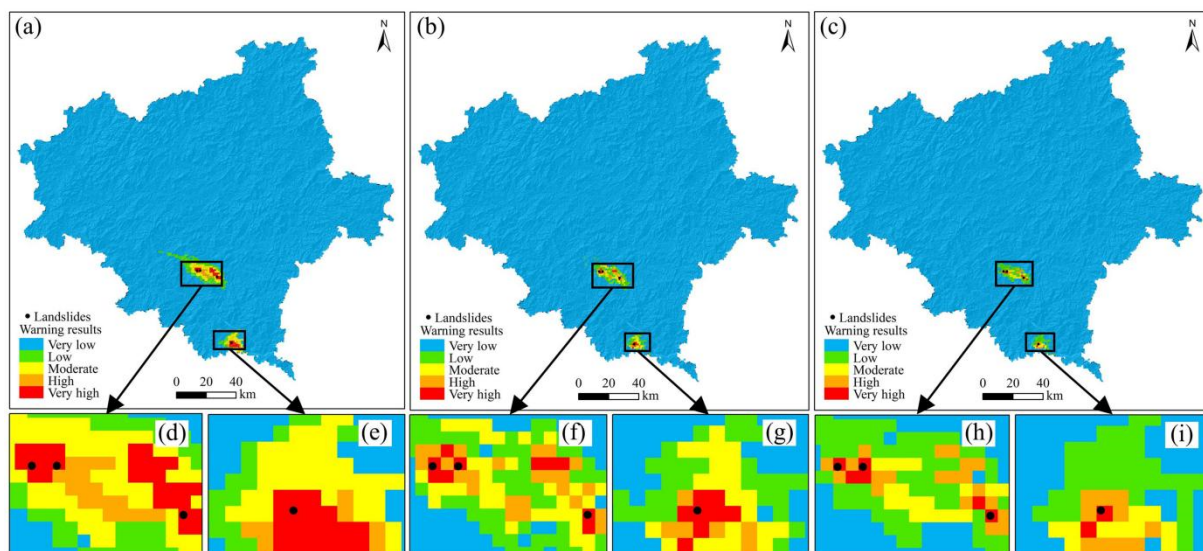


Fig. 11 Landslide warning results of 15:00 on May 31, 2021. (a) the rainfall threshold model; (b) the matrix coupled model; (c) the proposed probability coupled model; (d, e, f, g, h, i) locally magnified pictures.

predictions. To show the advantages of the proposed probability-coupled model, a rainfall process that triggered four landslides at approximately 15:00 on 31 May 2021 in Nanping was analyzed. The warning results obtained at 15:00 on 31 May 2021 from three different models, namely, the rainfall threshold model, the matrix-coupled model and the probability-coupled model, are shown in Fig. 11. The rainfall threshold model utilizes only the temporal probability of landslides, as shown in Fig. 2. The matrix-coupled model, which most previous studies have utilized, has classified the warning levels of rainfall thresholds and LS assessments. To compare the results of the probability-coupled model, five classes, e.g., four cutoff percentages (90%, 50%, 20% and 1%), were used. The LSI values were classified using a manual classifier into five categories. According to this classification method, more than 84% of landslides could be captured by the “very high” or “high” susceptibility warning level classes (Table 3). In this study, the matrix-coupled model determined warning levels based on a mixed matrix rather than providing continuous quantitative landslide probabilities (Fig. 12).

The prediction accuracies of the three models were evaluated using the “landslide hit index” (LHI) parameter:

$$LHI = \frac{L_W}{A_W} \# \tag{9}$$

where L_W is the number (or area) of landslides hit by a warning zone and A_W is the area of the warning zone. For a regular grid, the area can be quantified by

counting the grid cells. A higher LHI value suggests that more landslides are predicted in a smaller warning zone, indicating a higher prediction accuracy. In this study, red (very high) and orange (high) level zones were considered warning zones. Although the warning zones provided by the three models all successfully predicted the four landslides used as case studies, the areas differed notably. The results showed that the numbers of cells in the warning zones output by the matrix-coupled model and the probability-coupled model were much lower than the number of cells in the warning zone produced by the rainfall

Table 3 Warning level classes of landslides susceptibility

| Warning level | Landslide susceptibility index (LSI) value interval | Percentage of | |
|---------------|---|------------------|------------|
| | | Susceptible area | Landslides |
| Very high | 20.08~46.50 | 8.94% | 25.69% |
| High | 15.70~20.07 | 52.31% | 58.44% |
| Moderate | 13.05~15.69 | 27.48% | 13.92% |
| Low | 11.03~13.04 | 7.49% | 1.34% |
| Very low | 0.47~11.02 | 3.78% | 0.61% |

| | | Susceptibility warning level | | | | |
|----------------------------------|-----------------------|------------------------------|----------|----------|----------|----------|
| | | Very High | High | Moderate | Low | Very Low |
| Rainfall threshold warning level | Emergency (90.1~100%) | Very High | High | Moderate | Low | Very Low |
| | Alarm (50.1~90%) | High | Moderate | Low | Very Low | Very Low |
| | Attention (10.1~50%) | Moderate | Low | Very Low | Very Low | Very Low |
| | Watch (1.1~10%) | Low | Very Low | Very Low | Very Low | Very Low |
| | Monitor (0~1%) | Very Low | Very Low | Very Low | Very Low | Very Low |

Fig. 12 Warning levels based on matrix coupled model.

threshold model (Fig. 11). The LHI values of the rainfall threshold, matrix-coupled, and probability-coupled models were 0.0494, 0.0816 and 0.1026, respectively (Table 4). From a quantitative point of view, the probability-coupled model exhibited 107.7% and 25.7% improvements in their predictive accuracies compared to the rainfall threshold and matrix-coupled models, respectively.

Table 4 Comparison of warning results at 15:00, on May 31, 2021 among rainfall threshold model, matrix coupled model and probability coupled model

| Warning model | Count of | | Landslide hit index (LHI) |
|---------------------------|----------------------------|--------------------------------------|---------------------------|
| | Grid cells of warning zone | Predicted landslides in warning zone | |
| Rainfall threshold model | 81 | 4 | 0.0494 |
| Matrix coupled model | 49 | 4 | 0.0816 |
| Probability coupled model | 39 | 4 | 0.1026 |

The probability-coupled model exhibited a 25.7% precision increase when predicting landslides compared to the matrix-coupled model. In the matrix-coupled model, the rainfall threshold and LS were first divided into several levels; then, a coupled warning matrix was constituted with the derived rainfall threshold and susceptibility levels. Probability distribution information is lost during the rainfall threshold and susceptibility level classification processes. Moreover, this classification process introduces subjectivity, thus influencing the reliability of the resulting landslide predictions. The proposed probability-coupled model adopts only one classification step, i.e., the final step that determines warning levels based on the landslide probability (P_L). Landslide predictions are provided by the proposed model through the use of rainfall threshold and susceptibility probability distribution information; thus, the proposed model can issue warnings with a higher precision than those obtained by previous models.

4.2 Analysis of the effect caused by factors

The proposed probability coupled model consists of the rainfall threshold model and the LS assessment obtained from the FR method. Both the I-D model and the FR method are statistical models, and the input

data, i.e., rainfall data and environmental factors, have a great impact on the warning result. The quality of rainfall data impacts the accuracy of the landslide warning model. High-precision data are critical for determining rainfall thresholds (Jiang et al. 2022).

In this study, the rainfall data and the geoenvironmental factors directly impacted the results of the I-D threshold model and the MFRM, respectively. Because the surface runoff derived from rainwater removes unstable soil particles, the slope is eroded (Bai et al. 2022). The relationship between elevation and landslides is usually related to human activities. The lower the altitude is, the more frequent and denser human activities are. Human activities will easily change the local geological environment and the stability of slopes, which will improve the probability of landslides (Sun et al. 2022).

The landslide frequency (LF) represents the proportion of landslides in this category, and the class frequency (CF) is the proportion of each category in the factor. The FR value represents the contribution of every geoenvironmental factor to the occurrence of landslides (Fig. 13). When the FR value of a class exceeds 1, this class has a positive contribution to the occurrence of landslides. In contrast, an FR value of less than 1 indicates a negative contribution to the occurrence of landslides. The terrain data, i.e., the elevation, slope angle, slope aspect and curvature data, can be derived from the DEM data, which did not need to be classified in MFRM. The geoenvironmental data, i.e., the lithology, soil thickness, geomorphic types and distance to faults data, were divided into different classes (Fig. 13). The geology and geomorphology also play an important role and constitute the major predisposing factor controlling landslides (Shankar et al. 2022). Since soil landslides account for 79.3% of the Nanping landslide inventory, concave slope and the soil thickness are favorable factors to increase the water content of the soil slope. Water content is one of the main inducing factors of soil landslides, which explains the high LF and FR of 7-10 m and 10-15 m in soil thickness (Fig. 13b). Rock weathering in the study area is strong due to the erosion of typhoons and rainstorms. The strength of granite, glutenite and mica quartz schist become low after rock weathering, making the slope unstable. Therefore, the LF and FR in these three classes are high (Fig. 13a). The undulating terrain in hilly areas and human activity may be the reason why the majority of landslides in Nanping are distributed

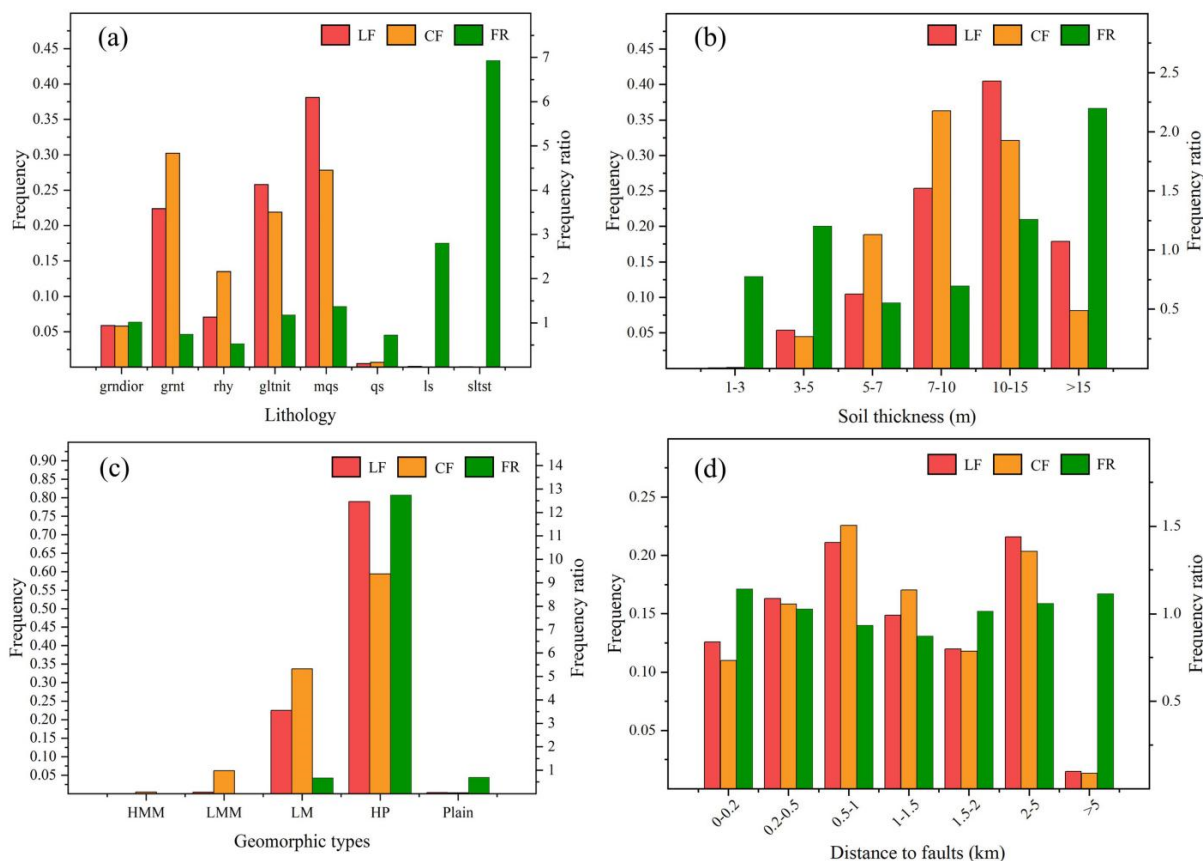


Fig. 13 Landslides frequency (LF, red bar), class frequency (CF, orange bar) and frequency ratio (FR, green bar) of each reclassified class in four geoenvironmental factors for LSM: (a) lithology (“grndior” means “granodiorite”, “grnt” means “granite”, “rhy” means “rhyolite”, “gltnit” means “glutenite”, “mqs” means “mica quartz schist”, “qs” means “quartz sandstone”, “ls” means “limestone”, “sltst” means “siltstone”); (b) soil thickness; (c) geomorphic (“HMM” means “high/medium mountain”, “LMM” means “low/medium mountain”, “LM” means “low mountain”, “HP” means “hilly plateau”) and (d) distance to faults.

in hilly plateaus with low elevations (Fig. 13c). The LR and FR in distance to faults vary little, which means that this factor makes little contribution to landslides in the study area (Fig. 13d). Some categories showed very high FR values, while the LF and CF values were too small. For example, the FR of siltstone in the lithology factor is the highest, while the LF and CF of siltstone are the lowest of all categories in lithology. This may be because the zone of siltstone occupies the smallest area, and a few landslides will cause a high FR value. Therefore, these special high FRs will not change the macroscopic distribution of regional landslide susceptibility assessment.

4.3 Real-time performance of the warning model

Landslide warning models usually require real-time performance with the premise of ensuring the effectiveness of the produced warnings. However,

some studies (Ahmed et al. 2018; Monsieurs et al. 2019) were only able to generate a daily warning result, which cannot meet the actual demand for landslide warning models.

The proposed probability-coupled model can fulfill the real-time requirements of landslide warning results. Some approaches adopted in the probability-coupled model serve to increase its computational efficiency. For instance, a reference rainfall duration equal to the maximum empirical effective rainfall duration was defined to allow the shortest possible rainfall records to be considered. A minimum cumulative rainfall threshold was also defined within the reference duration according to the historical rainfall record in the study area, so calculations were not performed at locations (grid cells) with nonsignificant rainfall less than the established threshold. This approach can drastically minimize the computational time required by the warning model. As the calculation of each cell is conducted completely

separately, the parallel method was used to speed up the model computing process. The perspective of this study was to also use rainfall forecasting to obtain a landslide early warning system.

The proposed model took just 15 min to provide landslide warning results covering the entirety of Nanping city (with an area of 26,300 km²) at a spatial resolution of 1 km × 1 km during the nonrainy season, while the computation time was twice as long or longer during the rainy season. The Raoba case study (Fig. 10) shows that the hourly warning results obtained using the proposed probability-coupled model could successfully meet the hourly real-time performance requirements. A very-high-level warning zone corresponding to the landslide location was successfully predicted an hour before the landslide occurrence (Fig. 10b).

4.4 Applicability in practice

The case study performed herein shows that the proposed probability-coupled model can satisfy the demands for landslide warning models in coastal regions of Southeast China, which is frequently affected by short-term heavy rainfall, in practice. The mitigation of landslide risks calls for the production of warnings as early as possible; thus, forecasted rainfall data can be utilized in the proposed model to calculate proactive real-time and hourly landslide warning results.

The proposed probability-coupled model can be easily applied to regions that are frequently impacted by heavy rainfall. Some preparations should be made before starting a similar application: (1) a detailed inventory of rainfall-induced landslides should be compiled to calculate the rainfall threshold; (2) the appropriate geoenvironmental factors should be selected for the LS assessment; and (3) precipitation data with the highest possible temporal and spatial resolutions should be collected.

The proposed probability-coupled model could be further improved by introducing automatic updates to the temporal and spatial probability distribution functions. The I-D relationship and LS map could be manually updated as new landslide events occur. The development of a completely automated module for updating the I-D relationship, LS map and their corresponding CDFs once the landslide inventory is updated would significantly improve the running efficiency of the model.

5 Conclusion

In this study, we proposed an hourly landslide warning model by coupling the temporal and spatial probabilities of landslides, which were calculated based on the rainfall threshold model and the LS model, respectively. The probability distribution of rainfall intensities that induced historical landslides was derived using the I-D threshold model and was then adopted to calculate the probability of a certain rainfall intensity triggering a landslide, i.e., the temporal probability of a landslide occurring. The landslide susceptibility probability distribution was obtained by the MFRM and was then used to calculate the probability that a landslide would occur in a certain location, i.e., the spatial landslide probability. Finally, the spatial and temporal landslide probabilities were multiplied to obtain the coupled landslide probability, and these probabilities were then classified into five levels to issue warning results.

The case study conducted herein shows that the proposed probability-coupled model can fully satisfy the accuracy, effectiveness, and hourly real-time performance requirements of landslide warnings. In terms of its quantitative precision, the probability-coupled model outperformed the rainfall threshold and matrix-coupled models by 107.7% and 25.7%, respectively. The proposed probability-coupled model is simple to implement and can be easily applied to other areas affected by rainfall-induced landslides. In further research, we will add forecasted rainfall data to the model to build a landslide early warning system. We believe that the proposed model in which the quantitative temporal and spatial landslide probabilities are coupled with real-time performance capabilities will positively contribute to local landslide risk mitigation.

Acknowledgments

This study was supported by the Strategic Priority Research Program of the Chinese Academy of Sciences (Grant No. XDA23090301), the National Natural Science Foundation of China (Grant No. 42041006 and 41927806), the Fundamental Research Funds for the Central Universities, CHD (Grant No. 300102262901).

References

- Adition A, Kubota T, Shinohara Y (2018) Comparison of GIS-based landslide susceptibility models using frequency ratio, logistic regression, and artificial neural network in a tertiary region of Ambon, Indonesia. *Geomorphology* 318: 101–111. <https://doi.org/10.1016/j.geomorph.2018.06.006>
- Ahmed B, Rahman M, Islam R, et al. (2018) Developing a dynamic web-GIS based landslide early warning system for the Chittagong metropolitan area, Bangladesh. *ISPRS Int J Geo-Inf* 7(12): 485. <https://doi.org/10.3390/ijgi7120485>
- Brunetti M, Melillo M, Gariano S, et al. (2021) Satellite rainfall products outperform ground observations for landslide prediction in India. *Hydrol Earth Syst Sci* 25(6): 3267–3279. <https://doi.org/10.5194/hess-25-3267-2021>
- Bai H, Feng W, Li S, et al. (2022) Flow-slide characteristics and failure mechanism of shallow landslides in granite residual soil under heavy rainfall. *J Mt Sci* 19(6): 1541–1557. <https://doi.org/10.1007/s11629-022-7315-8>
- Caine N (1980) The Rainfall Intensity - Duration Control of Shallow Landslides and Debris Flows, *Geograf Ann: Ser A, Phys Geogr* 62:1-2, 23–27. <https://doi.org/10.1080/04353676.1980.11879996>
- Cachon J, Irigaray C, Fernandez T (2006) Engineering geology maps: landslides and geographical information systems. *Bull Eng Geol Environ* 65:341–411. <https://doi.org/10.1007/s10064-006-0064-z>
- Choieta J, Oh HJ, Lee HJ., et al. (2012) Combining landslide susceptibility maps obtained from frequency ratio, logistic regression, and artificial neural network models using ASTER images and GIS. *Eng Geol* 124:12–23. <https://doi.org/10.1016/j.enggeo.2011.09.011>
- Corominas J, van Westen, Frattini P, et al. (2014) Recommendations for the quantitative analysis of landslide risk. *Bull Eng Geol Environ* 73:209–263. <https://doi.org/10.1007/s10064-013-0538-8>
- Chen W, Pourghasemi, Hamid Reza, et al. (2017) Spatial prediction of landslide susceptibility using an adaptive neuro-fuzzy inference system combined with frequency ratio, generalized additive model, and support vector machine techniques. *Geomorphology* 297:69–85. <https://doi.org/10.1016/j.geomorph.2017.09.007>
- Chapi K, Singh V, Shirzadi A, et al. (2017) A novel hybrid artificial intelligence approach for flood susceptibility assessment. *Environ Model & Soft* 95:229–245. <https://doi.org/10.1016/j.envsoft.2017.06.012>
- Ciccarese G, Mulas M, Corsini A (2021) Combining spatial modelling and regionalization of rainfall thresholds for debris flows hazard mapping in the Emilia-Romagna Apennines (Italy). *Landslides*, 2021, 18(11): 3513–3529. <https://doi.org/10.1007/s10346-021-01739-w>
- Di Napoli M, Carotenuto F, Cevasco A, et al. (2020) Machine learning ensemble modelling as a tool to improve landslide susceptibility mapping reliability. *Landslides* 17(8): 1897–1914. <https://doi.org/10.1007/s10346-020-01392-9>
- Floris M., Bozzano F (2008) Evaluation of landslide reactivation: a modified rainfall threshold model based on historical records of rainfall and landslides. *Geomorphology* 94(1-2): 40–57. <https://doi.org/10.1016/j.geomorph.2007.04.009>
- Froude and Petley (2018) Global fatal landslide occurrence from 2004 to 2016. *Nat Hazards Earth Syst Sci*, 2018, 18(8): 2161–2181. <https://doi.org/10.5194/nhess-18-2161-2018>
- Giannecchini R (2005) Rainfall triggering soil slips in the southern Apuan Alps (Tuscany, Italy). *Adv Geosci*, 2005, 2: 21–24. <https://doi.org/10.5194/adgeo-2-21-2005>
- Guzzetti F, Carrara A, Cardinali M, et al. (1999) Landslide hazard evaluation: a review of current techniques and their application in a multi-scale study, Central Italy. *Geomorphology* 31:181–216. [https://doi.org/10.1016/S0169-555X\(99\)00078-1](https://doi.org/10.1016/S0169-555X(99)00078-1)
- Guzzetti F, Peruccacci S, Rossi M, et al. (2007) The rainfall intensity–duration control of shallow landslides and debris flows: an update. *Landslides* 5(1):3–17. <https://doi.org/10.1007/s10346-007-0112-1>
- Guzzetti F, Gariano S, Peruccacci S, et al. (2020) Geographical landslide early warning systems. *Earth-Sci Rev*, 200: 102973. <https://doi.org/10.1016/j.earscirev.2019.102973>
- Ghobadi M, Nouri M, Saedi B, et al. (2017) The performance evaluation of information value, density area, LNRF, and frequency ratio methods for landslide zonation at Miandarband area, Kermanshah Province, Iran. *Arab J Geosci*, 2017, 10(19): 1–15. <https://doi.org/10.1007/s12517-017-3202-y>
- Huang Y, Zhao L (2018) Review on landslide susceptibility mapping using support vector machines. *Catena* 165: 520–529. <https://doi.org/10.1016/j.catena.2018.03.003>
- Hong H, Tsangaratos P, Ilia I, et al. (2020) Introducing a novel multi-layer perceptron network based on stochastic gradient descent optimized by a meta-heuristic algorithm for landslide susceptibility mapping. *Sci Tot Environ*, 2020, 742: 140549. <https://doi.org/10.1016/j.scitotenv.2020.140549>
- Iverson R (2000) Landslide triggering by rain infiltration. *Water Resour Res*, 36(7):1897–1910. <https://doi.org/10.1029/2000WR900090>
- Jenkinson A (1955) The frequency distribution of the annual maximum (or minimum) values of meteorological events. *Quart J Roy Meteorol Soc* 87(348):158–171. <https://doi.org/10.1002/qj.49708134804>
- Jaafari A, Najafi A, Pourghasemi HR, et al. (2014) GIS-based frequency ratio and index of entropy models for landslide susceptibility assessment in the Caspian forest, northern Iran. *Int J Environ Sci Tech* 11(4): 909–926. <https://doi.org/10.1007/s13762-013-0464-0>
- Jiang W, Chen G, Meng X, et al. (2022) Probabilistic rainfall threshold of landslides in Data-Scarce mountainous Areas: A case study of the Bailong River Basin, China. *Catena* 213: 106190. <https://doi.org/10.1016/j.catena.2022.106190>
- Ju NP, Huang J, Huang RQ, et al. (2015) A Real-time monitoring and early warning system for landslides in Southwest China. *J Mt Sci* 12(5): 1219–1228. <https://doi.org/10.1007/s11629-014-3307-7>
- Kayastha P, Dhital M, De Smedt (2012) Landslide susceptibility mapping using the weight of evidence method in the Tinau watershed, Nepal. *Nat Hazards* 63:479–498. <https://doi.org/10.1007/s11069-012-0163-z>
- Komolvilas V, Tanapalungkorn W, Latcharote P, et al. (2021) Ailure analysis on a heavy rainfall-induced landslide in Huay Khab Mountain in Northern Thailand. *J Mt Sci* 18(10):2580–2596. <https://doi.org/10.1007/s11629-021-6720-8>
- Lan H, Wu F, Zhou C, et al. (2003a) Spatial hazard analysis and prediction on rainfall-induced landslide using GIS. *Chin Sci Bull*, 48(7): 703–708. <https://doi.org/10.1007/BF03325659>
- Lan H, Zhou C, Lee C, et al. (2003b) Rainfall-induced landslide stability analysis in response to transient pore pressure-A case study of natural terrain landslide in Hong Kong. *Sci In Chin Ser E-Tech Sci* 46:52–68. <https://doi.org/10.1360/03ez0018>
- Lan H, Zhou C, Wang L (2004) Landslide hazard spatial analysis and prediction using GIS in the Xiaojiang watershed, Yunnan, China. *Eng Geol*, 76(1-2): 109–128. <https://doi.org/10.1016/j.enggeo.2004.06.009>
- Lan H, Li L, Zhang Y, et al. (2013) Risk assessment of debris flow in Yushu seismic area in China: a perspective for the reconstruction. *Nat Hazards Earth Syst Sci*, 2013, 13(11): 2957–2968. <https://doi.org/10.5194/nhess-13-2957-2013>
- Lan H, Peng J, Zhu Y, et al. (2021) Research on geological and surficial processes and major disaster effects in the Yellow River Basin. *Sci Chin Earth Sci*, 2021: 1–23. <https://doi.org/10.1007/s11430-021-9830-8>
- Liao M, Wen H, Yang L (2022) Identifying the essential

- conditioning factors of landslide susceptibility models under different grid resolutions using hybrid machine learning: A case of Wushan and Wuxi counties, China. *Catena*, 2022, 217: 106428. <https://doi.org/10.1016/j.catena.2022.106428>
- Li L, Lan H, Guo C, et al. (2017) A modified frequency ratio method for landslide susceptibility assessment. *Landslides*, 14(2): 727-741. <https://doi.org/10.1007/s10346-016-0771-x>
- Li L, Lan H (2020) Integration of Spatial Probability and Size in Slope-Unit-Based Landslide Susceptibility Assessment: A Case Study. *Int J Environ Res Public Health* 17(21): 8055. <https://doi.org/10.3390/ijerph17218055>
- Marchi L, Arattano M, Deganutti (2002) Ten years of debris-flow monitoring in the Moscardo Torrent (Italian Alps). *Geomorphology*, 2002, 46(1):1-17. [https://doi.org/10.1016/S0169-555X\(01\)00162-3](https://doi.org/10.1016/S0169-555X(01)00162-3)
- Monsieurs E, Dewitte O, Demoulin A (2019) A susceptibility-based rainfall threshold approach for landslide occurrence. *Nat Hazards Earth Syst Sci* 19(4): 775-789. <https://doi.org/10.5194/nhess-19-775-2019>
- Ma J, Xia D, Guo H, et al. (2022) Metaheuristic-based support vector regression for landslide displacement prediction: a comparative study. *Landslides* 19(10): 2489-2511. <https://doi.org/10.1007/s10346-022-01923-6>
- Ozturk D, Uzel-Gunini N (2022) Investigation of the effects of hybrid modeling approaches, factor standardization, and categorical mapping on the performance of landslide susceptibility mapping in Van, Turkey. *Nat Hazards*, 2022: 1-34. <https://doi.org/10.1007/s11069-022-05480-y>
- Pradhan S, Lee S, Kim Y (2019) A shallow slide prediction model combining rainfall threshold warnings and shallow slide susceptibility in Busan, Korea. *Landslides* 16(3): 647-659. <https://doi.org/10.1007/s10346-018-1112-z>
- Reichenbach P, Rossi M, Malamud B, et al. (2018) A review of statistically-based landslide susceptibility models. *Earth-sci rev*, 180: 60-91. <https://doi.org/10.1016/j.earscirev.2018.03.001>
- Roy J, Saha S, Arabameri A, et al. (2019) A novel ensemble approach for landslide susceptibility mapping (lsm) in Darjeeling and Kalimpong districts, West Bengal, India. *Remote Sens* 11(23):2866. <https://doi.org/10.3390/rs11232866>
- Rosi A, Segoni S, Canavesi V, et al. (2021) Definition of 3D rainfall thresholds to increase operative landslide early warning system performances. *Landslides*18(3): 1045-1057. <https://doi.org/10.1007/s10346-020-01523-2>
- Segoni S, Rossi G, Rosi A, et al. (2014) Landslides triggered by rainfall: a semi-automated procedure to define consistent intensity-duration thresholds. *Comput Geosci* 63: 123-131. <https://doi.org/10.1016/j.cageo.2013.10.009>
- Segoni S, Lagomarsino D, Fanti R, et al. (2015) Integration of rainfall thresholds and susceptibility maps in the Emilia Romagna (Italy) regional-scale landslide warning system. *Landslides* 12(4): 773-785. <https://doi.org/10.1007/s10346-014-0502-0>
- Segoni S, Tofani V, Rosi A, et al. (2018a) Combination of rainfall thresholds and susceptibility maps for dynamic landslide hazard assessment at regional scale. *Front in Earth Sci* 6: 85. <https://doi.org/10.3389/feart.2018.00085>
- Segoni S, Piciullo L, Gariano S L (2018b) A review of the recent literature on rainfall thresholds for landslide occurrence. *Landslides*, 15(8): 1483-1501. <https://doi.org/10.1007/s10346-018-0966-4>
- Stähli M, Sättele M, Huggel C, et al. (2015) Monitoring and prediction in early warning systems for rapid mass movements. *Nat Hazards Earth Syst Sci*, 15(4): 905-917. <https://doi.org/10.5194/nhess-15-905-2015>
- Sharma S, Mahajan A (2018) A comparative assessment of information value, frequency ratio and analytical hierarchy process models for landslide susceptibility mapping of a Himalayan watershed, India. *Bull Eng Geol Environ* 78(4): 2431-2448. <https://doi.org/10.1007/s10064-018-1259-9>
- Sala G, Lanfrancini C, Frattini P, et al. (2021) Cost-sensitive rainfall thresholds for shallow landslides. *Landslides*, 2021, 18(9): 2979-2992. <https://doi.org/10.1007/s10346-021-01707-4>
- Sun D, Gu Q, Wen H, et al. (2022) A Hybrid Landslide Warning Model Coupling Susceptibility Zoning and Precipitation. *Forests*, 2022, 13(6): 827. <https://doi.org/10.3390/f13060827>
- Shankar R, Satyam G, Singh P, et al. (2022) Impact of geomorphometric parameters on the occurrence and distribution of landslides in Yamuna River Basin, North-Western Himalaya, India. *J Mt Sci*, 2022: 1-23. <https://doi.org/10.1007/s11629-021-7081-z>
- Torizin J, Schüßler N, Fuchs M (2022) Landslide Susceptibility Assessment Tools v1.0.0 b-Project Manager Suite: a new modular toolkit for landslide susceptibility assessment. *Geosci Model Devel*, 2022, 15(7): 2791-2812. <https://doi.org/10.5194/gmd-15-2791-2022>
- Vakhshoori V, Zare M (2016) Landslide susceptibility mapping by comparing weight of evidence, fuzzy logic, and frequency ratio methods. *Geomatics, Nat Hazards Risk* 7(5): 1731-1752. <https://doi.org/10.1080/19475705.2016.1144655>
- Wu Y, Lan H, Gao X, et al. (2015) A simplified physically based coupled rainfall threshold model for triggering landslides. *Eng Geol*, 2015, 195: 63-69. <https://doi.org/10.1016/j.enggeo.2015.05.022>
- Wang Q, Wang D, Huang Y, et al. (2015) Landslide susceptibility mapping based on selected optimal combination of landslide predisposing factors in a large catchment. *Sustainability*, 2015, 7(12): 16653-16669. <https://doi.org/10.3390/su71215839>
- Wei L, Huang C, Chen H, et al. (2018) Adopting the I 3-R 24 rainfall index and landslide susceptibility for the establishment of an early warning model for rainfall-induced shallow landslides. *Nat Hazards Earth Syst Sci*, 18(6): 1717-1733. <https://doi.org/10.5194/nhess-18-1717-2018>
- Youssef, Pourghasemi H, Pourtaghi Z, et al. (2016) Landslide susceptibility mapping using random forest, boosted regression tree, classification and regression tree, and general linear models and comparison of their performance at Wadi Tayyah basin, Asir region, Saudi Arabia. *Landslides*, 2016, 13(5): 839-856. <https://doi.org/10.1007/s10346-015-0614-1>
- Zhang Y, Lan H, Li L, et al. (2020) Optimizing the frequency ratio method for landslide susceptibility assessment: A case study of the Caiyuan Basin in the southeast mountainous area of China. *J Mt Sci*, 17(2): 340-357. <https://doi.org/10.1007/s11629-019-5702-6>
- Zhang Y, Chen J, Wang Q, et al. (2022) Geographic information system models with fuzzy logic for susceptibility maps of debris flow using multiple types of parameters: a case study in Pinggu District of Beijing, China. *Nat Hazards Earth Syst Sci*, 2022, 22(7): 2239-2255. <https://doi.org/10.5194/nhess-22-2239-2022>